# Experimental evidence of flow destabilization in a two-dimensional bidisperse foam

I. Cantat,* C. Poloni, and R. Delannay
*GMCM, UMR 6626, Université de Rennes (CNRS), 263, av. du Général Leclerc 35042 Rennes Cedex, France*
(Received 29 October 2004; published 27 January 2006)

Liquid foam flows in a Hele-Shaw cell were investigated. The plug flow obtained for a monodisperse foam is strongly perturbed in the presence of bubbles whose sizes are larger than the average bubble size by an order of magnitude, at least. Above a velocity threshold, the large bubbles migrate faster than the mean flow. We evidence experimentally this instability and, in the case of a single large bubble, we compare the large bubble velocity to the prediction deduced from scaling arguments. In the case of a bidisperse foam, an attractive interaction between large bubbles induces segregation and the large bubbles organize themselves in columns oriented along the flow.

DOI: 10.1103/PhysRevE.73.011505 PACS number(s): 83.50.Ha, 82.70.Rr, 83.60.La

## I. INTRODUCTION

The rheology of two-dimensional foams is the object of renewed interest to elucidate the behavior of complex and structured fluids. In these materials, the subtle interplay between the elastic, plastic, and viscous behaviors induces complex rheological properties. The similarities between fluid foam, pastes, clays, or slurries arise from the organization at small scale of a disordered structure that governs the macroscopic behavior. In the case of foams, this small scale is the millimetric bubble scale, which is much easier to observe than the molecular scale usually involved. The structure determination is especially convenient in two-dimensional (2D) foam, which is thus often used as a model system for complex fluids [1–4].

We developed an experimental setup enabling foams to flow in a large 2D channel where dissipative processes are important. The foam is confined between two horizontal glass plates separated by a small gap, allowing a sole bubble layer to form. The whole films network, as well as the velocity fields, can thus be determined from images taken from above, where bubbles appear as polygons of various areas. Each vertical film touches both plates along lines called *plateau borders*. When sliding on the plates, they induce a viscous dissipation that becomes important even at relatively small velocities [5,6]. When a foam is pushed in the cell, it is thus subject to a viscous force depending on its velocity and on the density of plateau borders, i.e., on the bubble sizes. If the foam is polydisperse, the largest bubbles experience a smaller drag (per unit foam surface in 2D) than the smallest ones and tend, therefore, to move faster than the mean flow. For other kinds of 2D foams, like Langmuir monolayers or bubble rafts floating on a liquid surface, the dominating dissipation is of a different nature and this instability probably does not occur. The resulting flow is difficult to quantify in the general case of a polydisperse foam. As a first step, we investigated the case of a single large bubble (LB) embedded in a sea of much smaller bubbles and the case of a bidisperse foam with a minority of large bubbles. These large bubbles, which play the role of defects (or holes) in the foam, can be produced *a posteriori* with a controlled size and position by vaporization of liquid films with a laser.

As in a viscous instability of an interface, the pressure gradient in the foam is higher in front of the hole than to the sides. A similar hole in a simple viscous liquid would move ahead for this reason. In a foam, the shear stress created by the different pressure gradients must exceed a yield stress. A threshold velocity is thus set by a competition between surface tension and dissipative forces. Only above this velocity, do the large bubbles begin to migrate through the smaller bubbles. This migration does not imply that films break; the process is based on elementary neighbors exchanges involving four bubbles called T1 events [7] (see Fig. 2). The flow destabilization presented in this paper is based on wall effects and should thus be more important at smaller scale and especially in the domain of microfluidics.

This enhanced role of the dissipation in flows of 2D foam with large bubbles has been predicted numerically, but is demonstrated here in experiments. We present the experimental setup in Sec. II and the qualitative flow behavior in Sec. III. In Sec. IV, we briefly recall the theoretical predictions obtained previously [8,9]. Section V is devoted to the relative velocity of a single large bubble in a monodisperse foam flow, which is the main result of this paper. Finally, in Sec. VI, we show that size segregation occurs in the case of several large bubbles and that these bubbles organize themselves in columns oriented in the flow direction.

## II. EXPERIMENTAL SETUP

Foams were prepared from a solution of SDS (3 g/L), dodecanol (0.01 g/L), and glycerol (0.05 L/L) in ultrapure water. As-prepared solutions were used within a period of 24 h. The surface tension is $\gamma = 31 \times 10^{-3}$ N/m and the bulk viscosity is $\eta = 1.1 \times 10^{-3}$ Pa s. The cell flow is made of two large horizontal glass plates ($l = 35$ cm $\times L = 170$ cm) separated by a gap $h = 2$ mm (Fig. 1). It is connected upstream to a vertical production cell, of the same width and thickness, containing the foaming solution. The gap thickness is set by a steel piece, on which the glass plates are simply clamped. The foam is produced by blowing nitrogen continuously at a

*Electronic address: isabelle.cantat@univ-rennes1.fr

 

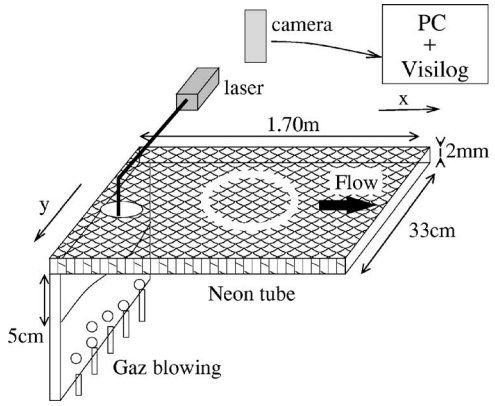


FIG. 1. Experimental setup.

controlled flow rate through four equally spaced needles of 1 mm diam. It drains in the vertical cell until it reaches the main cell (Fig. 1). The present data were collected with a drainage height of 5 cm. The resulting liquid fraction is difficult to estimate but it corresponds to a very dry foam. The plateau border size is typically $<0.5$ mm, and the observable interference patterns on both plates betray the presence of a micrometric wetting film.

Depending on the imposed gas flow rate, the turbulence in the foaming solution is modified and yields various polydispersities. We worked with almost monodisperse foams with a typical bubble volume of $V=5\times10^{-2}$ mL (which gives a typical diameter of $d=5\pm1$ mm for the polygons), obtained at the small flow rate of 1.5 mL/s per injector. The large bubble (LB) is produced by a YAG laser (wavelength 1064 nm, energy per pulse 20 mJ, pulse duration 5 ns). The beam is successively focused on each desired film with an orientable lens, until a bubble 10–400 times larger in volume is produced. Once the foam and the defect are produced at low flux, the foam flow is accelerated at the required velocity by increasing the gas flow rate. Velocities were varied between 0.3 and 10 cm/s. The structure of the foam produced at this stage may be highly disordered, but it does not influence the flow observed downstream.

The foam is lit laterally by a circular neon tube of diameter 0.4 m, set horizontally just below the cell on a black board. The plateau border network reflects the light at 90° and thus appears from above in white on a black background (see Fig. 2). Only the plateau borders perpendicular to the incident light lead to a good contrast and the isotropy of the light is thus crucial. The camera is placed above the middle of the cell, and the large bubble shape then has time enough to relax, spontaneously, from its initial arbitrary shape before reaching the recording zone. We record 25 images per second with a Pulnix TM6CN camera, with a resolution of $570\times760$ pixels. Images are processed using the Visilog commercial software to isolate each bubble and determine its area $a$ and center of mass. The polygon area $a$ is related to the bubble volume $V$ through the relation $V=ha$. The image processing consists of the following operations: we subtract the background to remove the large-scale heterogeneities of lightning and obtain binary images by thresholding (liquid is white and gas is black). Then a white pixel dilatation improves the bubble separation, and the resulting continuous

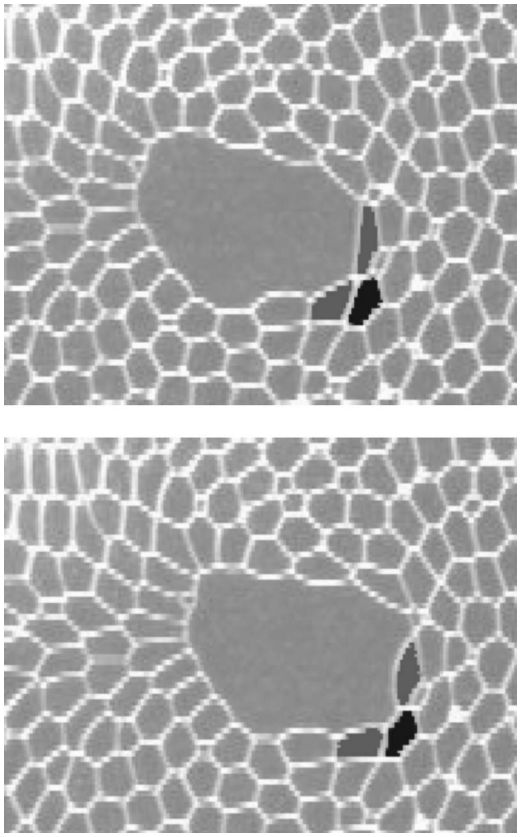

FIG. 2. Details of the raw images obtained from the camera. The foam, lit laterally by a circular neon tube, appears in white on a black background. The mean flow is oriented to the right, and the two images are separated by 120 ms. Small bubbles have a typical size of $d=5$ mm. The large bubble is migrating through the smallest ones due to T1 events: one of these elementary plastic transformations occurs between images (a) and (b), and the involved bubbles are underlined with a darker gray level.

white network is skeletized to a continuous frontier around each black bubble of one pixel width. The last step is to record the area and the center of mass of these connex domains of back pixels. Bubble tracking between images $n$ and $n+1$ is then performed. A bubble $k$ in image $n$ is identified with the bubble $k'$ in image $n+1$ if its center of mass (computed in image $n$) belongs to $k'$ in image $n+1$. We manually checked the pairing method on a few images and found that the error ratio was less than a few percent; thus, the individual bubble trajectories are determined with a good precision.

The dissipation in the foam is mainly due to the viscous forces between the glass plates and the plateau borders. The viscous force per unit plateau border length is predicted by the lubrication theory to be

$$\mathbf{f}_v \sim -\gamma \mathrm{Ca}^{\alpha}\mathbf{u}_x, \tag{1}$$

with $\mathrm{Ca}=\eta v_0/\gamma$ the capillary number, $v_0\mathbf{u}_x$ the plateau border velocity and $\alpha$ an exponent that is 2/3 in the limit of wet foam and mobile surfactants [5,10] and that varies roughly between 0.5 and 0.7 in the general case [11]. For the present foaming solution and in the velocity range investigated, we

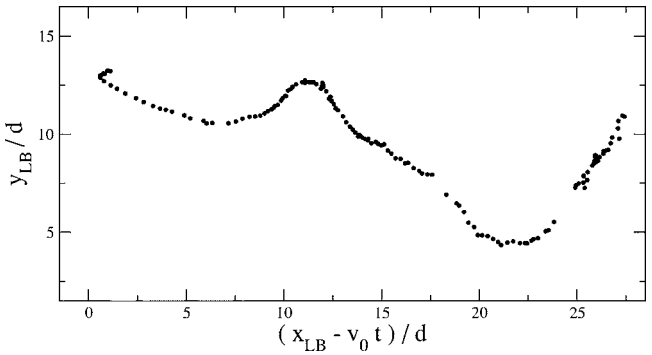


FIG. 3. Large bubble trajectory through the network of small bubbles, in the frame moving with the mean velocity of the foam $v_0\mathbf{u}_x$. $(x_{\mathrm{LB}},y_{\mathrm{LB}})$ is the LB position measured in the laboratory frame. The foam velocity is larger than the velocity threshold and the large bubble moves in the $x$ direction with a velocity fluctuating in amplitude and direction. Each dot corresponds to an image, separated by 40 ms.

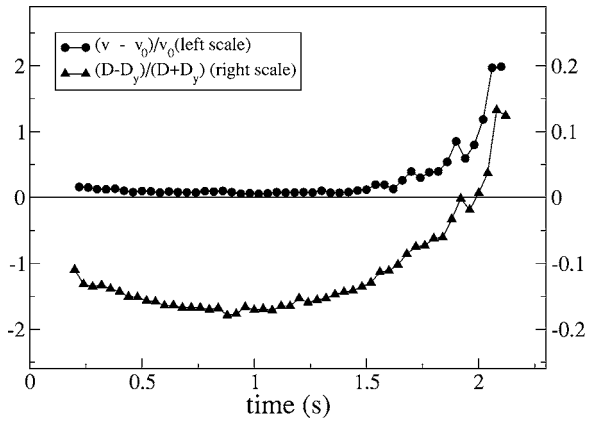


FIG. 4. The large bubble velocity $v$ is compared to the average flow velocity $v_0$, and correlated to the large bubble shape (the LB diameters in the $x$ and $y$ directions are, respectively, $D$ and $D_y$). An elongated shape oriented across the flow (large $D_y$) gives rise to a plug flow $(0<t<1.5)$. This shape may spontaneously destabilize $(1.5<t<2)$: a tip grows downstream in the flow direction, similarly to a viscous digitation. The tip finally contains the whole LB, which is then oriented along the flow $(t>2)$. This transformation coincides with an acceleration of the large bubble.

measured $\alpha=0.5\pm0.05$ with the technique detailed in [6]. These viscous forces are simply balanced by the pressure field, which thus scales, in a monodisperse foam of typical bubble diameter $d$, as

$$P(x) \sim -x\gamma \mathrm{Ca}^{\alpha}/(hd). \tag{2}$$

The total pressure gap $\Delta P$ between upstream and downstream was measured with a pressure sensor set in the foaming solution. For a flow velocity $v_0=3.2\times10^{-2}$ m/s and a small bubble size $d=5\times10^{-3}$ m, we measured $\Delta P=2800$ Pa, leading the typical viscous force per unit length of plateau border $f_v=h\Delta Pd/(2L)\sim10^{-2}$ N/m, in good agreement with previously obtained data [6].

## III. QUALITATIVE BEHAVIOR

The flow is obtained with a controlled foam flux. At the velocity range of interest, the first bubble layer on both sides slips on the wall at the mean velocity. In monodisperse foam, topological transformations are thus very rare and the foam structure remains almost unchanged during the flow. The instantaneous velocity distribution is well fitted by a Gauss distribution with a standard deviation of the order of ±5%, due to the pixelization. In contrast, in the presence of a large bubble, the plug flow becomes unstable above a given foam velocity. The large bubble velocity is then larger than the mean flow velocity $v_0$, with important amplitude fluctuations and an orientation that may vary between ±30° with respect to the mean flow direction (see Fig. 3). The large bubble shape was characterized by its diameters in the direction of the flow $D(t)$ and in the transverse direction $D_y(t)$. These two parameters depend on time, in contrast with the LB area, which is constant. The LB velocity is strongly correlated to the bubble elongation $(D-D_y)/(D+D_y)$ that varies roughly between $-1/2$ and $1/2$. The large bubble alternates periods, during which it moves much faster than typical bubbles, with a shape elongated in the direction of its own relative motion, and periods during which it moves at the average speed with an elongated shape perpendicular to the mean flow (see Fig. 4).

The large bubble migration occurs without films breakages. Small bubbles are separated in front of the large bubble and are reconnected at the rear. These so-called T1 events, depicted in Fig. 2, are mainly localized very close to the large bubble, but many structure reorganizations are also induced much further, in the whole camera field. The velocity field around the large bubble may exhibit very different behaviors. Indeed, the presence of a wake of small bubbles behind the large one is intermittent. Comparison to foams flowing around an obstacle of fixed shape would thus be very interesting to perform [12].

## IV. THEORETICAL PREDICTIONS

This instability was already studied numerically and theoretically in [8,9]. We summarize here the theoretical predictions for the large bubble velocity. The scaling behavior of the threshold is obtained from the expression of the various forces acting on the large bubble. From the pressure field given in Eq. (2), we obtain the resulting pressure force on LB,

$$F_d \sim D^2(\gamma/d)\mathrm{Ca}^{\alpha}, \tag{3}$$

which is the driving force for the LB migration. For simplicity, we only retain in the model a single diameter $D$ for the large bubble. Below the threshold, the LB equilibrium thus results from a competition between the pressure field pushing LB downstream (the driving force $F_d$) and the surface tension force of the soap films network that try to keep LB at its initial position in the foam frame. At small deformations, this force $F_e$, due to the fact that any modification of the foam structure increases the total amount of interfaces (and

then of energy), is well predicted by a purely elastic model [13]. This leads to

$$F_e \sim \gamma h X/d, \tag{4}$$

with $\gamma/d$ the order of magnitude of the foam shear modulus [7] and $X$ the LB displacement with respect to its equilibrium position. This expression is obtained from a continuous incompressible 2D elastic medium at rest at infinity. In this case, the force exerted on a circular obstacle, indeed, scales as the obstacle displacement time the material shear modulus (up to disregarded corrections, depending logarithmically on $D/l$ with $l$ the cell width).

The local elastic stress $\sigma$ is related to $F_e$ by $F_e=\sigma L_{\text{geo}}h$, with $L_{\text{geo}}h$ the typical area on which the stress is important around the front or the rear of LB. This length scale $L_{\text{geo}}$ is probably related to the shape curvature around the front of the large bubble, and its value will be estimated later, from the experimental results. At the instability threshold, this local stress reaches the plastic threshold of the foam, scaling as $\gamma/d$ [13]. The force balance on the large bubble is then, from Eq. (3), $D^2(\gamma/d)\text{Ca}^{\alpha}\sim\gamma L_{\text{geo}}h/d$ or, equivalently, with $v_{\text{th}}$ the velocity threshold,

$$\eta v_{\text{th}}/\gamma \sim (hL_{\text{geo}}/D^2)^{1/\alpha}. \tag{5}$$

Above this threshold, the large bubble begins to migrate, with a mean velocity $v$ modelized by the following process. The instantaneous LB velocity $v(t)$ decreases during the elastic loading of the foam until the plastic threshold is reached. Then T1 events occur, and a new cycle begins. A full stress relaxation is assumed after each plastic event, and the elastic force is zero. Between two plastic events, the elastic force is obtained from Eq. (4), $F_e=\gamma h/d\int_0^t(v(t')-v_0)dt'$. The integral is the LB displacement $X$ with respect to the small bubble network, since the last plastic relaxation, occurring at $t=0$.

The viscous force exerted on the plateau border around LB is finally, from Eq. (1), of the order of $D\gamma(\eta v(t)/\gamma)^{\alpha}$, leading to the force balance

$$\frac{\gamma h}{d}\int_0^t (v(t')-v_0)dt' - \frac{D^2\gamma}{d}\left(\frac{\eta v_0}{\gamma}\right)^{\alpha} + D\gamma\left(\frac{\eta v(t)}{\gamma}\right)^{\alpha} = 0. \tag{6}$$

The first term is the elastic force given above, the second is the driving force [Eq. (3)], and the third is the viscous force. This integral equation has been solved analytically in the general case in [9]. When $\alpha=1$ and $D\gg d$, we obtain for the LB mean velocity $v$ the simple expression given below. It differs only by a few percent from the general expression for reasonable values of $\alpha$ and $D/d$. Thus, we use it for simplicity (see Fig. 5)

$$\frac{v-v_0}{v_0\dfrac{D}{d}} \sim \frac{-v_{\text{th}}/v_0}{\ln\left(1-\dfrac{v_{\text{th}}}{v_0}\right)}. \tag{7}$$

When $v_0\gg v_{\text{th}}$, the expression becomes asymptotically $(v-v_0)/(v_0D/d)=1$, or equivalently $v=v_0D/d$ as $D\gg d$ [8].

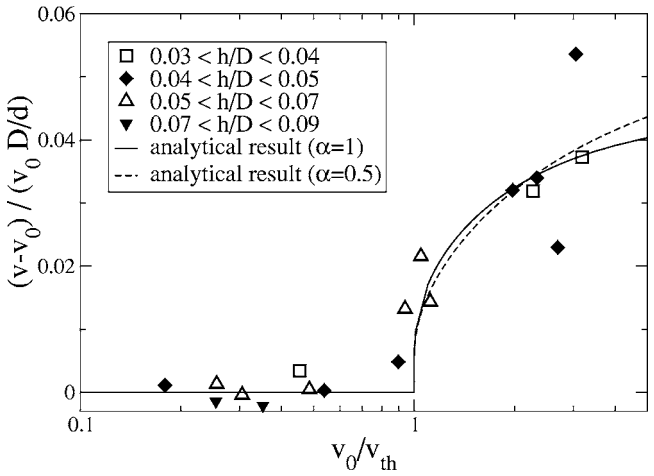


FIG. 5. Large-bubble relative velocity in rescaled units (same data as in Fig. 7). The mean flow velocity threshold $v_{\text{th}}(D)$ used to rescale the experimental data, is obtained from Eq. (8). The first analytical result (full line) is obtained from Eq. (7), with the adjustable prefactor 0.045. Numerical simulations using the vertex model have been performed (see [9]), leading to a good agreement with theory as well, with an adjustable prefactor of 0.07 of the same order. The second curve (dashed line) is the exact solution of Eq. (6), using the experimental value of $\alpha$ ($\alpha=0.5$), with an adjustable prefactor (see [9]).

Equations (5) and (7) are used to rescale the experimental data.

## V. EXPERIMENTAL RESULTS

The aim of the present paper is to experimentally determine the relation, at each time, between the LB velocity in the flow direction, denoted by $v(t)$, the mean flow velocity $v_0$ and the large bubble size characterized by its diameter in the $x$ direction $D(t)$, which appeared to be the pertinent size parameter.

We analyzed 56 movies with a large bubble remaining 2 or 3 s in the view field. All control parameters were kept constant, except for the LB area and the mean flow velocity $v_0$. The measured values of $v(t)$ and $D(t)$ were averaged over five images. When $v(t)>1.1v_0$, a flow is considered as being above the threshold, otherwise it is below. All experimental points are represented in the plane $(h/D, \eta v_0/\gamma)$ on Fig. 6. Despite relatively large fluctuations, two distinct domains clearly appear on this phase diagram, corresponding to the two states, namely, above or below the threshold (only the parameter ranges near the threshold were investigated).

To compare the experimental data presented in Fig. 6 with the theoretical prediction given by Eq. (5), we adjust the experimental frontier by minimizing the distances $d_{\text{front}}$ between the graph of a function and the experimental points located on the "wrong" side of this frontier. We use a least-squares method with the set of functions $f(x)=ax^b$, $a$ and $b$ being free parameters. We obtain the relation

$$\eta v_{\text{th}}/\gamma = 68(h/D)^{3.7}. \tag{8}$$

The mean value of $d_{\text{front}}$ increases by 10% if the exponent varies of ±0.5, which is the order of the precision on the

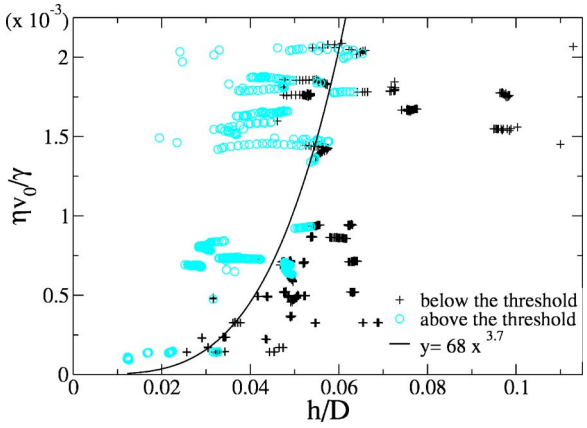


FIG. 6. (Color online) Phase diagram of the large bubble instability. The control parameters are the capillary number built with the mean flow velocity $\mathrm{Ca}=\eta v_0/\gamma$ and the LB diameter $D$ adimensioned by the gap $h$ between the plates. Each point of the graph corresponds to an image, on which the large bubble is migrating (circle) or not (cross). Despite large fluctuations, a frontier between the stable and unstable domains in the $(h/D,\mathrm{Ca})$ plane can be determined. The full line is the best fit of this frontier in power law, $ax^b$ with $a$ and $b$ adjustable.

exponent. This very crude estimation is, nevertheless, sufficient to discriminate between the two possible scaling for $L_{\mathrm{geo}}$. Indeed, $L_{\mathrm{geo}}=D$ in Eq. (5) would correspond to an exponent 2 in Eq. (8) (with $\alpha=0.5$), whereas $L_{\mathrm{geo}}=d$ leads to the relation

$$\eta v_{\mathrm{th}}/\gamma \sim (d/h)^2(h/D)^4, \tag{9}$$

which agrees better with Eq. (8). We would need more experimental data to confirm the value of this exponent, but $h$ cannot be easily varied in our setup and $d$ is confined to the small value range $h<d\ll D\ll l$, with $l$ the channel width. Nevertheless, this suggests that $L_{\mathrm{geo}}\sim d$. Further modeling will account more precisely for deformations of the large bubble during the flow. The discrete nature of the foam especially influences the LB geometry in the high-stress regions. The direct determination of the stress and strain from the image, using the tensors introduced by Aubouy *et al.* would also allow one to improve the comparison between experimental and theoretical approachs [14].

Above the threshold, the large bubble migrates through the foam with a velocity $v(t)>v_0$. Experimentally, the foam disorder induces large fluctuations of $v$ (depicted in Fig. 3), which have been averaged out. The averages were performed over small bins of size $\delta(\eta v_0/\gamma)=0.25\times10^{-3}$ and $\delta(h/D)=0.01$ or 0.02, leading to the graphs presented in Fig. 7. As expected, the large-bubble velocity, in the frame of the foam, is vanishing at small foam velocity and/or small LB size. It can reach $0.5v_0$ (i.e., $1.5v_0$ in the laboratory frame) for the largest foam flux explored. At larger velocities, images are not recorded fast enough by our camera to extract quantitative results. Other physical processes, such as film breakages, are involved and modify the dynamical behavior. For very large bubbles, the shape remains no more convex. The description of the phenomena in term of a Saffman Taylor instability is then probably more appropriate [15,16].

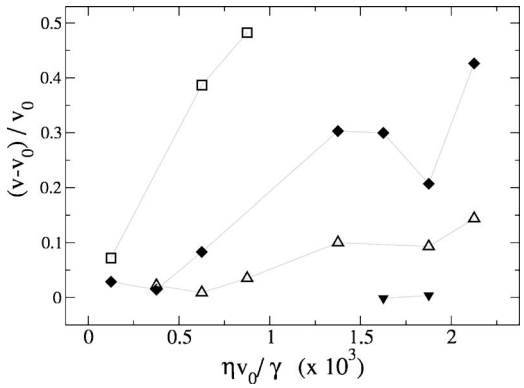


FIG. 7. Large-bubble relative velocity $(v-v_0)/v_0$ as a function of the mean foam velocity $v_0$, for different large-bubble size $D$ (the $h/D$ ratios are given in Fig. 5 with the same symbol convention). Each point represents an average over few tens of measures.

The experimental data shown in Fig. 7 were rescaled according to the theoretical prediction Eq. (7). The value used for the velocity threshold is the experimental fit given by Eq. (8). In that way, we obtain a good superposition of curves for the various $h/D$ values, as well as an agreement with the theory (see Fig. 5).

The problem of the orientation of the LB velocity remains open. Local crystallization is presumably important, as shown numerically. By contrast, disorder induces randomized plastic thresholds in the foam and, thus, creates most favorable paths for the LB migration that may deviate from a straight line. A precise analysis of the coupling between the local foam structure, the T1 localization, and the LB shape and orientation might help to clarify these questions.

## VI. LARGE-BUBBLE SEGREGATION IN BIDISPERSE FOAM

Polydisperse foam flows imply obvious interactions between bubbles of various sizes. A mean-field approach, in which we would consider that each bubble migrates in an effective continuous medium and adjusts its velocity as a function of its own size and of the local mean velocity and mean bubble size does not seem appropriate. The flow appears indeed to be dominated by correlations between

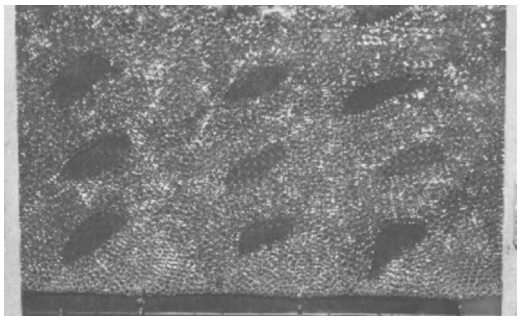

FIG. 8. Initial structure of the bidisperse foam.

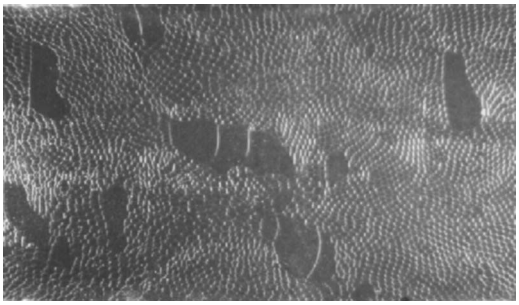

FIG. 9. Picture of the same foam as in Fig. 8, taken few seconds later, 50 cm downstream in the cell. The foam flow is oriented to the right. Some of the ten large bubbles have spontaneously organized in a few bubble columns oriented along the flow. A few bubbles of intermediate size are due to a few undesirable film breakages and are disregarded.

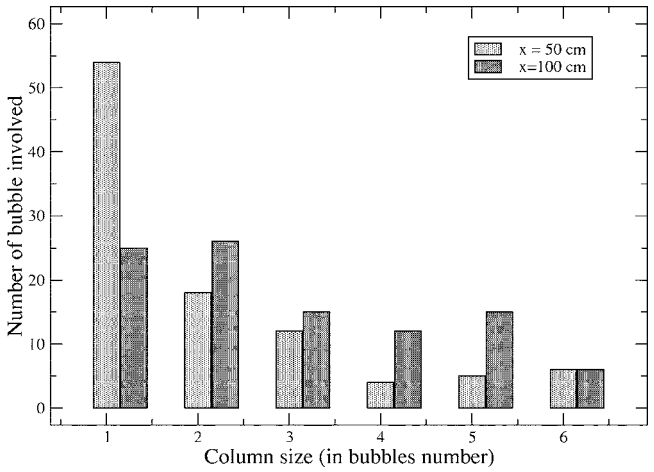


FIG. 10. Large-bubble repartition in the columns of various sizes, at two abscissa in the cell. Ten flows have been recorded, involving 99 large bubbles. The position $x=0$ corresponds to the mean abscissa of the initial regular large bubble network (see Fig. 8). Each time a large bubble crosses the line $x=50$ cm (resp. $x=100$ cm), the size of the column in which this bubble migrates is recorded (size 1 corresponds to an isolated large bubble) and the obtained distribution is plotted. The count is focused on the bubbles, which number is conserved, and the $n$-bubble columns are thus counted $n$ times.

bubbles. In this last part, we point out the attractive interactions between a set of large bubbles and their spontaneous organization in columns.

A regular network of approximately ten large bubbles is initially produced in a monodisperse foam, at rest (Fig. 8). The middle of this network is used as abscissa reference ($x=0$). Then the flow is turned on, at a velocity higher than the threshold, and the large bubbles begin to migrate through the foam. When two large bubbles meet, they migrate together. This aggregation leads progressively to large-bubble domains of increasing size, organized in one-bubble-width columns, oriented along the flow (see Fig. 9). The length of the columns was measured at two points along the flow, for ten flows (99 bubbles). The number $N(n)$ of bubbles involved in a $n$-bubble column when crossing the abscissas $x=50$ or $x=100$ cm is plotted for each value of $n$ in Fig. 10 ($n=1$ for an isolated bubble). This represents, equivalently, the number of $n$-bubble columns, with a weight $n$. The initial distribution at $x=0$ is simply $N(1)=99$ and $N(i)=0$ for $i>1$. In order to follow every large bubble, we needed a large field of view. The image quality is therefore reduced, and the analysis was done by hand.

The number of isolated bubbles decreases along the flow. The aggregation process may be due to long-range attractive forces or simply due to the spontaneous fluctuations of the large-bubble trajectories, coupled to a short-range adhesion. The orientation of the domains is probably governed by the same phenomenon as in viscous digitation.

## VII. CONCLUSION

Our experiments demonstrated the crucial role of polydispersity in non-quasi-static foam flows. We measured the relative velocity of a single large bubble created in a monodisperse foam as a function of its size and of the mean flow velocity. The results are explained with scaling arguments. In a bidisperse foam, we show that large bubbles are attracted to each other and organize themselves in columns oriented along the flow. In future, a more refined analysis of the velocity fields around these large bubbles should yield a better understanding of the nature of the attractive interaction. Strong spatial correlations are observed, and a mean-field approach is probably not enough to explain the velocity field of a fully polydisperse foam.

The dissipation is of different nature in three-dimensional (3D) foams. Nevertheless, it is still localized in the liquid phase, and the largest bubbles remain easier to deform or displace. The investigation of similar destabilizations in non-quasi-static 3D flows is, thus, an interesting open question that might have important practical consequences.

## ACKNOWLEDGMENTS

We thank Rennes Métropole and CNRS for financial support, P. Chasles and S. Bourlès for technical assistance and valuable advice, and G. Le Caër and B. Dollet for enlightening discussions.

[1] M. A. Fortes and M. E. Rosa, J. Phys.: Condens. Matter **11**, 7947 (1999).
[2] G. Debregeas, H. Tabuteau, and J.-M. diMeglio, Phys. Rev. Lett. **87**, 178305 (2001).
[3] J. Lauridsen, M. Twardos, and M. Dennin, Phys. Rev. Lett. **89**, 098303 (2002).
[4] M. Asipauskas, M. Aubouy, J. A. Glazier, F. Graner, and Y. Jiang, Granular Matter **5**, 71 (2003).
[5] G. Hirasaki and J. B. Lawson, Soc. Pet. Eng. J. p. 176 (1985).
[6] I. Cantat, N. Kern, and R. Delannay, Europhys. Lett. **65**, 726 (2004).
[7] D. Weaire and S. Hutzler, *The Physics of Foams* (Oxford Uni-

versity Press, London, 2000).
[8] I. Cantat and R. Delannay, Phys. Rev. E **67**, 031501 (2003).
[9] I. Cantat and R. Delannay, Eur. Phys. J. E **18**, 55 (2005).
[10] F. P. Bretherton, J. Fluid Mech. **10**, 166 (1961).
[11] N. D. Denkov, V. Subramanian, D. Gurovich, and A. Lips, Colloids Surf., A **263**, 129 (2005).
[12] B. Dollet, F. Elias, C. Quilliet, C. Raufaste, M. Aubouy, and F. Graner, Phys. Rev. E **71**, 031403 (2005).
[13] D. Weaire and M. A. Fortes, Adv. Phys. **43**, 685 (1994).
[14] M. Aubouy, Y. Jiang, J. A. Glazier, and F. Graner, Granular Matter **5**, 67 (2003).
[15] S. S. Park and D. J. Durian, Phys. Rev. Lett. **72**, 3347 (1994).
[16] A. Lindner, P. Coussot, and D. Bonn, Phys. Rev. Lett. **85**, 314 (2000).